

Translocator protein as an imaging marker of macrophage and stromal activation in RA pannus

Nehal Narayan*¹, David R Owen², Harpreet Mandhair¹, Erica Smyth³, Francesco Carlucci¹, Azeem Saleem³, Roger N Gunn³, Eugenii A. Rabiner^{3,4}, Lisa Wells³, Stephanie G Dakin¹, Afsie Sabokbar^{§1}, Peter C. Taylor^{§1}.

*= corresponding author

§= joined senior authors

¹Nuffield Department of Orthopaedics Rheumatology and Musculoskeletal Sciences, University of Oxford, Headington, Oxford, UK, OX3 7HE. ²Division of Brain Sciences, Imperial College, Hammersmith, London, UK, W12 0NN. ³Imanova Centre for Imaging Sciences, Hammersmith, London, UK, W12 0NN. ⁴Centre for Neuroimaging Sciences, Institute of Psychiatry, Psychology and Neuroscience, King's College, London, UK

corresponding author address (and address for reprints):

Nehal Narayan, Nuffield Department of Orthopaedics Rheumatology and Musculoskeletal Sciences, Botnar Research Centre, University of Oxford, Headington, Oxford, UK, OX3 7HE, e-mail: nehal.narayan@ndorms.ox.ac.uk, tel: 01865 227 374.

Nehal Narayan is currently a DPhil student and Rheumatology medicine SpR trainee in the West Midlands, UK.

Word count (from start of title page to refs): 6063.

FUNDING STATEMENT

NN, AS, PCT: The research was supported by the National Institute for Health Research (NIHR) Oxford Biomedical Research Centre (BRC). The views expressed are those of the authors and not necessarily those of the NHS, the NIHR or the Department of Health. NN was also supported by an IMPETUS pilot study

grant from Imanova, Academic Centre for Imaging Sciences. DO is funded by an MRC clinician scientist award (MR/N008219/1). SGD is funded by an Oxford UCB Prize Fellowship in Biomedical Sciences and also received funding from Arthritis Research UK (20506).

CONFLICTS OF INTEREST:

The authors declare no conflicts of interest regarding this work.

Running head: TSPO in RA pannus

ABSTRACT

Positron Emission Tomography (PET) radioligands targeted to Translocator protein (TSPO), offer a highly sensitive and specific means of imaging joint inflammation in rheumatoid arthritis (RA). Through high expression of TSPO on activated macrophages, TSPO PET has been widely reported in several studies of RA as a means of imaging synovial macrophages *in vivo*. However, this premise does not take into account the ubiquitous expression of TSPO. This study aimed to investigate TSPO expression in major cellular constituents of RA pannus; monocytes, macrophages, fibroblast-like synoviocytes (FLS) and CD4+ T lymphocytes, to more accurately interpret TSPO PET signal from RA synovium.

Methods: 3 RA patients and 3 healthy volunteers underwent PET both knees using the TSPO radioligand ^{11}C -PBR28. Through synovial tissue ^3H -PBR28 autoradiography and immunostaining of 6 RA patients and 6 healthy volunteers, cellular expression of TSPO in synovial tissue was evaluated. TSPO mRNA expression and ^3H -PBR28 radioligand binding was assessed using *in vitro* monocytes, macrophages, FLS and CD4+ T-lymphocytes.

Results: ^{11}C -PBR28 PET signal was significantly higher in RA compared to healthy joints (average SUV 0.82 ± 0.12 compared to 0.03 ± 0.004 respectively, $p < 0.01$). Further, ^3H -PBR28 specific binding in synovial tissue was approximately 10-fold higher in RA compared to healthy controls. Immunofluorescence revealed TSPO expression on macrophages, FLS and CD4+ T cells. *In vitro* study demonstrated

highest *TSPO* mRNA expression and ³H-PBR28 specific binding, in activated FLS, non-activated and activated 'M2' reparative macrophages, with least *TSPO* expression in activated and non-activated CD4+ T lymphocytes.

Conclusion: This study is the first evaluation of cellular *TSPO* expression in synovium, finding highest *TSPO* expression and PBR28 binding on activated synovial FLS and M2 phenotype macrophages. *TSPO* targeted PET may therefore have unique sensitivity to detect FLS and macrophage predominant inflammation in RA, with potential utility to assess treatment response in trials using novel FLS-targeted therapies.

Key words: fibroblast-like synoviocytes, macrophages, translocator protein, positron emission tomography.

Rheumatoid Arthritis is a common inflammatory arthritis, affecting up to 1% of the population(1). Imaging is recognized as a useful tool to aid early diagnosis of RA, thus preventing permanent joint damage and disability (2, 3). Musculoskeletal imaging is also used to assess response to treatment, for individual patients in clinical practice (4), and in clinical trials, to better ascertain which experimental therapy is sufficiently effective to progress to use in clinical practice. Through a unique ability to image a desired molecular target *in vivo*, PET has potential to be a highly sensitive and specific imaging tool for the detection and quantification of synovitis in RA.

The mitochondrial membrane protein TSPO (translocator protein), of as yet uncertain function, is reportedly highly expressed on activated macrophages (5, 6). Macrophages are well established to have a key role in RA pathogenesis; with synovial sublining staining for these cells known to correlate with disease activity (7, 8) and joint destruction (9, 10). To date, the TSPO targeted PET radioligand ¹¹C-PK11195, has been used as a purported imaging tool for synovial macrophages, capable of detecting and quantifying not only clinically apparent RA synovitis (11), but subclinical synovitis in those with RA in clinical remission (12).

Inflamed synovium in RA consists of a 'pannus', made up of multiple cells, with major groups including macrophages, activated stromal cells (FLS), and CD4+T lymphocytes, which can make up to 30-50% of pannus cells (13-15). Since TSPO is ubiquitously expressed (5), it cannot be assumed that TSPO PET signal in RA

synovium is solely due to presence of macrophages. Studies comparing TSPO expression in different RA pannus cell types, are lacking. Hence, major cellular contributor(s) of TSPO PET signal in RA pannus remain unclear.

The TSPO radioligand ^{11}C -PBR28 is known to have superior TSPO signal than the first generation TSPO ligand ^{11}C -PK11195 (16, 17), where high background signal is recognized as a limitation to its use (18). Here, through ^{11}C -PBR28 PET-Computed Tomography (CT) imaging of RA patients and healthy volunteers, we provide evidence that ^{11}C -PBR28 signal reflects presence of RA pannus. Using ^3H -PBR28 synovial tissue autoradiography and corresponding histological studies, we investigate whether ^3H -PBR28 binding reflects TSPO expression in synovium, and which cells in synovial tissue express TSPO. Real-Time PCR, and radioligand binding studies provide quantitative evidence of TSPO expression in major cellular components of pannus at mRNA and protein level, examining TSPO expression in unstimulated, and activated, CD4+ T lymphocytes, monocytes, macrophages, and FLS. Given current uncertainty of macrophage phenotypes in RA synovium, macrophages at both ends of the spectrum of macrophage phenotypes (pro-inflammatory ('M1') and reparative ('M2') macrophages (19)) were assessed in this work.

PATIENTS AND METHODS

Patient recruitment

Ethical approval was granted by West London and GTAC Research Ethics Committee (ref: 15/LO/0013). All participants gave written informed consent. Three patients (2 male, 1 female; age range 40-54 years), with established RA (as per ACR criteria (20)) and clinical evidence of synovitis in one or both knees, along with 3 healthy control participants (all male, age range 38-65 years), with no history of arthritis, underwent ^{11}C -PBR28 PET-CT of both knees. Previous knee surgery was an exclusion criterion for participants undergoing ^{11}C -PBR28 PET-CT. Supplemental table 1 details age and medications of RA patients undergoing imaging.

***rs6971* genotyping**

Whilst second generation TSPO radioligands, such as ^{11}C -PBR28 offer specific signal and robust quantification(16), target binding affinity is affected by a single nucleotide polymorphism in the *TSPO* gene (*rs6971*) (21). To ensure results from *in vivo* imaging, autoradiography and radioligand binding were comparable between donors, only those carrying two copies of the common allele ('high affinity binders') were included in this work. Genotyping was performed as previously described using peripheral whole blood (21).

^{11}C -PBR28 PET-CT

^{11}C -PBR28 PET-CT was carried out in Imanova Centre for Academic Imaging Sciences, London, UK. ^{11}C -PBR28 radioligand synthesis and quality checks were performed as described previously (18). Approximately 400mBq ^{11}C -PBR28, was administered as a peripheral intravenous bolus over 20 seconds at the start of a 90-minute dynamic PET acquisition (Siemens Biograph 6 PET-CT scanner, SIEMENS, Knoxville, TN) of both knees for RA participants, with static scan both knees at 50 minutes post radioligand administration for healthy controls.

PET data were reconstructed using filtered back projection, correcting for attenuation and scatter. Regions of interest (ROI) were defined by outlining anatomical location of synovium using CT as a guide. ROI were applied to the ^{11}C -PBR28 data to generate mean voxel radioactivity for the full duration of the scan. Time activity curves for the full duration of the scan were corrected for radioactive decay and normalized for injected radioactivity. Semi-quantitative standardized uptake values (SUV) for radioactivity over 50-70 minutes post radioligand injection were calculated by dividing radioactivity in the ROI by radioactivity of ligand injected per kg patient body weight (22).

Synovial tissue acquisition

Synovial knee tissue was obtained from ultrasound guided biopsy of three RA patients undergoing ^{11}C -PBR28 both knees as previously described (23). Three further RA patients undergoing knee joint replacement surgery, who did not

undergo ^{11}C -PBR28 both knees, also provided synovial tissue. Healthy control synovial tissue was provided from patients undergoing knee arthroscopy for ligamentous knee injury. Specimens from each donor were placed *en bloc* in Leica[®] OCT, and snap frozen in isopentane (-70°C) prior to sectioning. All tissue provided were from high affinity binder donors. Supplemental table 1 details age and medications of RA patients providing synovial tissue.

Sectioning

Frozen blocks were serially sectioned using a cryostat microtome (Leica, Wetzlar, Germany; CM1900) across adjacent slides at thickness of $10\mu\text{m}$ for autoradiography, as described previously by Owen *et al.* (24). For immunostaining work, tissue was serially sectioned at $5\mu\text{m}$ thickness onto Leica[®] Xtra adhesive slides. Sections were stored at -80°C until use. For autoradiography, tissue was used within 21 days of sectioning.

Autoradiography

Autoradiography binding was performed using protocols previously described (24) on sectioned synovial tissue using optimised experimental conditions judged from *in vitro* ^3H -PBR28 binding studies. At least 3 synovial tissue sections from each donor were placed on one slide. One synovial tissue section was considered as an ROI, and average values for each ROI were converted to $\text{fmol } ^3\text{H}\text{-ligand/mg wet}$

tissue equivalent using the calibrated ^3H -microscale standards. Specific binding of ^3H -PBR28 in synovium was calculated from subtracting average non-specific binding from total ^3H -PBR28 binding on tissue autoradiography of serial sections of synovial tissue for each donor, determining mean specific binding component.

Immunohistochemistry and Immunofluorescence

List of antibodies, dilutions used and isotype negative control images are detailed in Supplemental table 2. For immunohistochemistry, sections were stained as described in Dakin *et al.* (25). Immunohistochemistry images were acquired on an inverted bright field microscope using Axiovision software (Zeiss). Twelve images were acquired in a systematic manner at x400 magnification with oil immersion by a single blinded investigator. Image analysis was performed using ImageJ (NIH) as described previously (26). For every sample, immunopositive staining was normalized to number of haematoxylin-counterstained nuclei within the field of view.

Co-staining of TSPO with other cell markers using immunofluorescence

For multiple antibody immunofluorescence staining and image acquisition, protocols were modified as per Dakin *et al.* (25). To provide confirmation of cell type, two established cell markers were used for each cell type; for macrophages, the less macrophage specific CD68, and more synovial macrophage specific

CD163 (27); for FLS, CD55 (also known as decay accelerating factor) and PDPN (podoplanin, gp38) (28), and for CD4⁺ T lymphocytes, CD3 and CD4, were employed. The acquisition of immunofluorescence images is described in Supplemental data.

In vitro cell culture studies

Monocytes were isolated from peripheral blood donor cones (National Blood Service, Colindale, London), using density dependent centrifugal elutriation, as previously described (29-31), to obtain fractions of 85% monocytes.

Differentiation of monocytes to macrophages was undertaken using 100ng/mL of recombinant human Macrophage Colony-Stimulating Factor (Peprotech Inc, UK) at a concentration of 1×10^6 monocytes/mL, for 7 days (32), as previously described in Narayan *et al.* (33). Fluorescence activated cell sorting was used to confirm monocytes had been differentiated to monocyte-derived macrophages (34).

On day 7, macrophages were treated with 10ng/mL Lipopolysaccharide (LPS) (Peprotech) and 20ng/mL recombinant human IFN- γ (Peprotech), for 24 hours to generate pro-inflammatory 'M1' phenotype macrophages. To generate reparative 'M2' phenotype macrophages, cells were treated with 20ng/mL IL-4 as described in previous studies (32, 35-37).

Lymphocytes were isolated through centrifugal elutriation as described above, generating fractions of 90% lymphocytes. CD4⁺ T-cells were isolated from

lymphocyte fractions using the positive selection CD4+ T-cell Isolation kit (Miltenyi, Bisley UK). CD4+ cells were left unstimulated, or treated with 10ng/mL phorbol 12-myristate 13-acetate plus 1µg/mL ionomycin for 6 hours (38).

FLS were isolated from arthroscopic biopsy of healthy human knee synovial tissue, through processing of tissue as previously described (39). *FLS* were stimulated with 10ng/mL TNF- α or 10ng/mL IL-1 β for 24 hours, or left unstimulated.

Real-time Quantitative Polymerase Chain Reaction

Methodology for RNA extraction, complementary DNA synthesis and Real-time quantitative polymerase chain reaction from cells used are described elsewhere (25). Two µL cDNA was used in a 10µL volume with Fast SYBR Green Master Mix (Applied Biosystems) and diluted validated primers (Invitrogen) for *TSPO* (forward 5'-GCGGCCTGGCTAACTCCTGC-3', reverse 5'-AAAGCGGGAGCCCACGAAGC-3') or the reference gene for human *18s* (forward 5'-GTAACCCGTTGAACCCCA-3', reverse 5'-CCATCCAATCGGTAGTAGCG-3'). *TSPO* mRNA data are shown normalized to *18s*.

Radioligand saturation binding

The protocol for radioligand saturation binding has been described in (24). Aliquots of cell protein (50µg protein/mL) were utilized for saturation analysis. For saturation analysis, eight concentrations of ³H-PBR28 were used, ranging from 0.1 nmol/L to 100 nmol/L. The specific binding component for ³H-PBR28 was defined by addition of unlabelled PK11195 (10 µmol/L). Each concentration was performed in triplicate. B_{\max} (fmol/mg protein) and K_d (nmol/L) values were determined using GraphPad Prism 5.0 software (GraphPad Software Inc., La Jolla, CA, USA). To calculate average fmol of ligand per cell, the number of mg of protein from preparation of each cell pellet was multiplied by the B_{\max} in fmol/mg.

Statistical Analysis

All data is presented as mean ± standard error of the mean. Statistical analysis was undertaken using GraphPad Prism 7 (GraphPad Software Inc., San Diego, CA). Normality was tested using a Kolmogorov-Smirnov test. Mann-Whitney U test was undertaken to assess comparisons of *in vivo* ¹¹C-PBR28 PET SUV signal, tissue autoradiography, and staining quantification between healthy and RA groups. Pearson's correlation was used to assess relationship between specific binding of ³H-PBR28 and TSPO staining. For mRNA and radioligand binding data, one way analysis of variance (ANOVA) was performed, followed by Bonferroni's Multiple Comparison Test, if more than two groups to compare, or Student *t*-test,

if two groups were compared. *P* values less than 0.05 were considered significant (**p*<0.05, ***p*<0.01, ****p*≤0.001).

RESULTS

In vivo ¹¹C-PBR28 signal in joints

¹¹C-PBR28 PET-CT demonstrated significantly higher SUV along the anatomical location of synovium in clinically inflamed knees of patients with RA compared to negligible SUV in healthy control knees (average SUV 0.82 ± 0.12 in RA patients, compared to 0.03 ± 0.004 for healthy knees; *p*<0.01, see **Fig. 1**).

³H-PBR28 synovial autoradiography, and relationship with synovial immunohistochemical TSPO staining

Non-specific binding was negligible in both RA and healthy tissue (see **Fig. 2B, 2C** for an example of non-specific binding and total binding in RA and healthy synovial tissue).

Specific binding of ³H-PBR28 in RA synovial tissue was approximately 10-fold higher than in healthy controls (1264 ± 58.9 fmol/mg in RA synovial tissue compared to 122.8 ± 22.5 fmol/mg in healthy tissue, see **Fig. 2D**).

Serial sections of RA and healthy control synovial tissue used for autoradiography, were immunohistochemically stained for TSPO (see **Fig. 3A** for a representative example). The average number of cells staining positive for TSPO on sections from each donor were calculated. Number of cells positive for TSPO were significantly higher in RA compared to healthy synovial tissue (**Fig. 3B**). A positive correlation ($r^2=0.99$, $p<0.001$) was also noted between specific binding of ^3H -PBR28 and average number of TSPO positive cells, in serial sections of synovial tissue from RA donors (**Fig. 3C**).

Immunofluorescence studies

Immunofluorescence staining of synovial tissue demonstrated co-expression of TSPO on cells expressing macrophage markers (CD68 and CD163) (**Fig. 4A**), FLS markers CD55 and PDPN (**Fig. 4B**), as well as cells expressing T lymphocyte markers, CD3 and CD4 (**Fig. 4C**). This provides *ex-vivo* evidence that TSPO is likely expressed on macrophages, fibroblasts, as well as CD4+ T lymphocytes in RA synovial tissue.

In vitro evidence of TSPO expression in cells of human pannus

In vitro studies were undertaken to quantify TSPO expression, and ^3H -PBR28 binding in major cell groups known to make up human pannus. The impact of cell activation on TSPO expression/ ^3H -PBR28 binding was also assessed.

As we previously describe in detail (33), differentiation of monocytes to non-activated macrophages (M0 macrophages) significantly increased *TSPO* mRNA expression by a fold change of 60.7 ± 2.38 ($p < 0.05$). Likewise, ^3H -PBR28 binding mirrored this significant increase, with specific binding ^3H -PBR28 of 1004 ± 52.61 fmol/ 1×10^6 cells for monocytes, increasing to 1838 ± 45.37 fmol/ 1×10^6 cells for M0 macrophages ($p < 0.01$) (**Fig. 5**) (33). Additionally, we previously describe that activation of macrophages to an M2 phenotype using IL-4 did not significantly increase *TSPO* expression at mRNA level, or ^3H -PBR28 binding (**Fig. 5, (33)**), yet both *TSPO* mRNA expression and ^3H -PBR28 binding were significantly downregulated on macrophages activated to an M1 phenotype, to levels not statistically dissimilar from monocytes (33).

The FLS activating cytokines, TNF- α or IL-1 β , also upregulated *TSPO* on FLS; *TSPO* mRNA expression significantly increased by a fold change of 2.33 ± 0.37 upon TNF- α stimulation ($p < 0.05$) and 2.84 ± 0.19 on IL-1 β stimulation ($p < 0.01$), compared with unstimulated FLS. Likewise, specific binding ^3H -PBR28 significantly increased from 1532 ± 196 fmol/ 1×10^6 cells for unstimulated FLS, to 2627 ± 180.4 fmol/ 1×10^6 cells for TNF- α stimulated cells ($p < 0.001$), and 2355 ± 153.4 fmol/ 1×10^6 cells for IL-1 β stimulated cells ($p < 0.01$) (**Fig. 5**).

In contrast, activation of CD4 $^+$ T lymphocytes with phorbol 12-myristate 13-acetate and ionomycin, *TSPO* expression did not significantly increase *TSPO* expression or ^3H -PBR28 binding (fold change mRNA expression of 1.10 ± 0.15 for

activated cells compared to 1 for non-activated, $p=0.55$, and specific binding of ^3H -PBR28 275.2 ± 30.67 fmol/ 1×10^6 cells for activated cells, compared to 128.6 ± 64.08 fmol/ 1×10^6 cells for non-activated, $p=0.99$) (**Fig. 5**).

TSPO mRNA expression (relative to mRNA expression in unstimulated CD4+T lymphocytes), was compared between all cells types in both unstimulated and activated states (**Fig. 6**). Highest *TSPO* mRNA expression was seen in activated FLS (fold change of 73.82 ± 7.31 for FLS activated with IL-1 β and 62.75 ± 10.03 for FLS activated with TNF- α), along with M2 macrophages and M0 macrophages (fold change 60.69 ± 2.38 , and 46.04 ± 5.19 , respectively (see **Fig. 6**).

Likewise, highest ^3H -PBR28 specific binding was seen in activated FLS (2355 ± 153.4 fmol/ 1×10^6 cells in FLS treated with IL-1 β , and 2627 ± 180.4 fmol/ 1×10^6 cells in FLS treated with TNF- α), along with non-activated M0 and M2 macrophages (^3H -PBR28 specific binding 1838 ± 45.37 and 2223 ± 143.6 fmol/ 1×10^6 cells, respectively). The next highest specific binding of ^3H -PBR28 was seen in monocytes, M1 macrophages and unstimulated FLS (^3H -PBR28 specific binding of 1004 ± 52.61 , 994.3 ± 21.93 and 1532 ± 196 fmol/ 1×10^6 respectively). The lowest ^3H -PBR28 binding was seen in CD4+ T lymphocytes (128 ± 64.08 fmol/ 1×10^6 cells) (see **Fig. 6**).

DISCUSSION

The utility of TSPO targeted PET as an imaging tool for inflammation, is based upon the notion of high TSPO expression on activated macrophages (5). The long-established role of macrophages in RA pathogenesis, has driven interest in using TSPO PET as a macrophage targeted imaging tool to detect and quantify RA synovitis *in vivo*. To date, several studies have demonstrated the ability of TSPO PET to detect and quantify RA joint inflammation, even at subclinical and pre-clinical stages (11, 12, 40, 41).

However, cell types other than macrophages also play a critical role in RA; the importance of T lymphocytes in RA is well established, as evidenced by the efficacy of the T cell targeted therapy abatacept for RA (42). Additionally, the role of FLS in RA pathogenesis is being increasingly realized (14), with a growing body of research aiming to identify appropriate FLS specific targets for RA therapies (28, 43).

Van der Laken *et al.* previously demonstrated that staining for the macrophage marker CD68, correlated with TSPO radioligand ^{11}C -PK11195 signal in RA joints (11), supporting the idea that TSPO PET signal is macrophage specific in RA pannus. However, it is recognized that CD68 is also expressed on FLS in RA pannus (44, 45), and additionally, TSPO expression is known to be ubiquitous (5). Hence, it cannot be assumed that TSPO is macrophage specific in synovium. In

this study, we aimed to better ascertain the major cellular contributors to TSPO PET signal in human RA pannus.

The second generation TSPO PET radioligand ^{11}C -PBR28 has high specificity for its target (18). We demonstrated that *in vivo* ^{11}C -PBR28 signal was significantly higher in RA compared to healthy control knee joints. Synovial tissue autoradiography confirmed significantly higher ^3H -PBR28 binding in RA synovial tissue compared to healthy, with a significant correlation of TSPO immunohistochemical staining with ^3H -PBR28 binding, confirming that PBR28 binding reflects synovial tissue TSPO expression, as well as the presence of RA pannus.

Immunofluorescence studies demonstrated co-staining of TSPO on cells expressing macrophage, FLS and CD4+ T lymphocyte markers, providing the first histology data indicating that TSPO appears to be expressed on all major cell types in RA pannus.

In vitro studies demonstrated least expression of TSPO in CD4+ T lymphocytes compared to monocytes as determined by mRNA and radioligand binding studies; in keeping with previous studies of peripheral blood leukocytes (46). However, previous data comparing TSPO expression on monocytes and macrophages is lacking; with this study confirming that TSPO is significantly upregulated on non-activated macrophages, compared to monocytes.

We previously describe that activation of macrophages to a more reparative M2 phenotype in the presence of IL-4 does not significantly alter TSPO expression (33), yet activation to a pro-inflammatory M1 phenotype (19), significantly downregulates both *TSPO* mRNA, and specific binding of ³H-PBR28. This finding is in keeping with a recent observation in the brain tissue of an infection induced mouse model of neuro-inflammation, where TSPO downregulation was observed in microglia in the presence of increased pro-inflammatory cytokine expression (47).

In contrast, activation of FLS, with TNF- α or IL-1 β , further increased *TSPO* mRNA expression and ³H-PBR28 binding, whereas activation of CD4+ T lymphocytes, did not impact upon *TSPO* expression. Given that the function of TSPO is currently uncertain, further *in vitro* study may lend insight into the role of TSPO in macrophage phenotype generation, as well as leukocyte and stromal activation, in RA pathogenesis.

Overall, ³H-PBR28 binding was highest in activated FLS, activated M2 and non-activated M0 macrophages, with significantly less binding in M1 macrophages, monocytes and unstimulated FLS, and least binding of TSPO in unstimulated and activated CD4+ T lymphocytes. Given the known prominence of synovial hyperplasia in RA due to FLS proliferation, it is feasible that a significant

contribution of TSPO PET signal will be from activated FLS, as well as macrophages.

Although participant number for this work was small, both histology and *in vitro* data confirmed expression of TSPO on all major cell groups in pannus, and *in vitro* data reached statistical significance. Due to need for a large amount of protein for radio-ligand binding studies, leukocytes were derived from healthy donors for *in vitro* cell work in this investigation. Therefore, it is plausible that TSPO expression patterns seen in this study might differ in cells from RA patients. Further, although stimuli applied to activate *in vitro* cells in this study are widely accepted, multiple, complex stimuli are likely to act on cells *in vivo*. Therefore, additional study of TSPO expression on cells directly extracted from RA synovium, in a larger patient cohort, would help to confirm findings from this study.

This work only assessed the expression of TSPO in the reportedly most abundant cell groups in pannus (13). However, multiple other cell groups also exist in pannus, including endothelial cells, and osteoclasts (13). The use of flow and mass cytometry studies, could enable assessment of TSPO expression in less abundant cells isolated directly from RA synovial tissue.

It must be acknowledged that although second generation TSPO radioligands, such as PBR28, have superior affinity and specificity for their target, the requirement for genotyping in order to interpret results may preclude their routine

use in clinical practice. However, they remain potentially highly useful research tools in assessing treatment response in early phase clinical trials.

Our findings that TSPO is expressed on all major cell groups found in RA pannus, could explain why TSPO PET has been demonstrated thus far, to be a highly sensitive indicator of synovitis, being superior to magnetic resonance imaging in detecting sub-clinical joint inflammation (41). The histological heterogeneity of RA synovial tissue is increasingly recognized, with cellular components differing between individuals regardless of disease activity, and also changing as the disease advances (48, 49). The fact that TSPO PET is able to detect all major cell groups of pannus means that the ability of this imaging technique to detect synovitis will not be dependent on a single pattern of synovial histology, hence potentially making it highly sensitive as an imaging technique. The fact that TSPO is expressed most highly in activated fibroblasts as well as M2 macrophages, may render TSPO targeted PET particularly useful for assessing response to treatment to potential FLS targeted therapies, a key new area of drug development in therapies for RA (28).

CONCLUSION

Our results suggest that TSPO PET radioligand binding in RA joints reflects cellularity and activation of inflammatory cells within RA pannus. The high contribution of activated FLS to TSPO PET signal, may lend utility to TSPO PET

as a tool for assessing treatment response to novel emerging synovial FLS targeted therapies for RA.

Using human RA and healthy volunteers, and synovial tissue, we confirmed that the TSPO radioligand PBR28 binds in RA pannus, with negligible signal in healthy joints and tissue. Immunofluorescence studies of RA synovium, and *in vitro* ³H-PBR28 binding studies confirmed TSPO presence on all major cell groups of pannus, with maximal *TSPO* mRNA expression and ³H-PBR28 binding in activated FL, and M2 'reparative' phenotype macrophages. Activation of macrophages to a pro-inflammatory 'M1' phenotype, significantly reduced *TSPO* mRNA expression and ³H-PBR28 binding.

The differential expression of TSPO on activated macrophages of different phenotype, whilst being upregulated in activated FLS, may provide further clues as to the role of TSPO in RA pathogenesis.

ACKNOWLEDGEMENTS

We thank patients from Nuffield Orthopaedic Centre Oxford Rheumatology Outpatients Department, for their participation in this work. Professor Hemant Pandit assisted in the acquisition of healthy synovial tissue for this work.

REFERENCES

1. Symmons D, Turner G, Webb R et al. The prevalence of rheumatoid arthritis in the United Kingdom: new estimates for a new century. *Rheumatology*. 2002;41:793-800.
2. Zeman MN, Scott PJ. Current imaging strategies in rheumatoid arthritis. *Am J Nucl Med Mol Imaging*. 2012;2:174-220.
3. Filer A, de Pablo P, Allen G et al. Utility of ultrasound joint counts in the prediction of rheumatoid arthritis in patients with very early synovitis. *Ann Rheum Dis*. 2011;70:500-7.
4. Colebatch AN, Edwards CJ, Ostergaard M et al. EULAR recommendations for the use of imaging of the joints in the clinical management of rheumatoid arthritis. *Ann Rheum Dis*. 2013;72:804-14.
5. Batarseh A, Papadopoulos V. Regulation of translocator protein 18 kDa (TSPO) expression in health and disease states. *Mol Cell Endocrinol*. 2010;327:1-12.
6. Papadopoulos V, Baraldi M, Guilarte TR et al. Translocator protein (18kDa): new nomenclature for the peripheral-type benzodiazepine receptor based on its structure and molecular function. *Trends Pharmacol Sci*. 2006;27:402-9.
7. Haringman JJ, Gerlag DM, Zwinderman AH et al. Synovial tissue macrophages: a sensitive biomarker for response to treatment in patients with rheumatoid arthritis. *Ann Rheum Dis*. 2005;64:834-8.

8. Tak PP, Smeets TJ, Daha MR et al. Analysis of the synovial cell infiltrate in early rheumatoid synovial tissue in relation to local disease activity. *Arthritis Rheumatol.* 1997;40:217-25.
9. Mulherin D, Fitzgerald O, Bresnihan B. Synovial tissue macrophage populations and articular damage in rheumatoid arthritis. *Arthritis Rheumatol.* 1996;39:115-24.
10. Tak PP, Bresnihan B. The pathogenesis and prevention of joint damage in rheumatoid arthritis: advances from synovial biopsy and tissue analysis. *Arthritis Rheumatol.* 2000;43:2619-33.
11. van der Laken CJ, Elzinga EH, Kropholler MA et al. Noninvasive imaging of macrophages in rheumatoid synovitis using ¹¹C-(R)-PK11195 and positron emission tomography. *Arthritis Rheumatol.* 2008;58:3350-5.
12. Gent YY, Ahmadi N, Voskuyl AE et al. Detection of subclinical synovitis with macrophage targeting and positron emission tomography in patients with rheumatoid arthritis without clinical arthritis. *J Rheumatol.* 2014;41:2145-52.
13. Tran CN, Lundy SK, Fox DA. Synovial biology and T cells in rheumatoid arthritis. *Pathophysiology.* 2005;12:183-9.
14. Bartok B, Firestein GS. Fibroblast-like synoviocytes: key effector cells in rheumatoid arthritis. *Immunol Rev.* 2010;233:233-55.
15. Firestein GS, Zvaifler NJ. How important are T cells in chronic rheumatoid synovitis? *Arthritis Rheumatol.* 1990;33:768-73.

16. Chauveau F, Boutin H, Van Camp N, Dolle F, Tavitian B. Nuclear imaging of neuroinflammation: a comprehensive review of [¹¹C]PK11195 challengers. *Eur J Nucl Med Mol Imaging*. 2008;35:2304-19.
17. Kobayashi M, Jiang T, Telu S et al. ¹¹C-DPA-713 has much greater specific binding to translocator protein 18 kDa (TSPO) in human brain than ¹¹C-(R)-PK11195. *J Cereb Blood Flow Metab*. March 21, 2017 (epub ahead of print).
18. Owen DR, Guo Q, Kalk NJ et al. Determination of [(¹¹C)]PBR28 binding potential in vivo: a first human TSPO blocking study. *J Cereb Blood Flow Metab*. 2014;34:989-94.
19. Murray PJ, Allen JE, Biswas SK et al. Macrophage activation and polarization: nomenclature and experimental guidelines. *Immunity*. 2014;41:14-20.
20. Aletaha D, Neogi T, Silman AJ et al. 2010 rheumatoid arthritis classification criteria: an American College of Rheumatology/European League Against Rheumatism collaborative initiative. *Ann Rheum Dis*. 2010;69:1580-8.
21. Owen DR, Yeo AJ, Gunn RN et al. An 18-kDa translocator protein (TSPO) polymorphism explains differences in binding affinity of the PET radioligand PBR28. *J Cereb Blood Flow Metab*. 2012;32:1-5.
22. Thie JA. Understanding the standardized uptake value, its methods, and implications for usage. *J Nucl Med*. 2004;45:1431-4.
23. Kelly S, Humby F, Filer A et al. Ultrasound-guided synovial biopsy: a safe, well-tolerated and reliable technique for obtaining high-quality synovial tissue

from both large and small joints in early arthritis patients. *Ann Rheum Dis.* 2015;74:611-7.

24. Owen DR, Howell OW, Tang SP et al. Two binding sites for [3H]PBR28 in human brain: implications for TSPO PET imaging of neuroinflammation. *J Cereb Blood Flow Metab.* 2010;30:1608-18.
25. Dakin SG, Martinez FO, Yapp C et al. Inflammation activation and resolution in human tendon disease. *Sci Transl Med.* 2015;7:311ra173-311ra173.
26. Franklin SL, Dean BJ, Wheway K, Watkins B, Javaid MK, Carr AJ. Up-regulation of Glutamate in Painful Human Supraspinatus Tendon Tears. *Am J Sports Med.* 2014;42:1955-62.
27. Fonseca JE, Edwards JC, Blades S, Goulding NJ. Macrophage subpopulations in rheumatoid synovium: reduced CD163 expression in CD4+ T lymphocyte-rich microenvironments. *Arthritis Rheumatol.* 2002;46:1210-6.
28. Filer A. The fibroblast as a therapeutic target in rheumatoid arthritis. *Curr Opin Pharmacol.* 2013;13:413-9.
29. Berger TG, Strasser E, Smith R et al. Efficient elutriation of monocytes within a closed system (Elutra) for clinical-scale generation of dendritic cells. *J Immunol Methods.* 2005;298:61-72.
30. Schwanke U, Nabereit A, Moog R. Isolation of monocytes from whole blood-derived buffy coats by continuous counter-flow elutriation. *J Clin Apher.* 2006;21:153-7.

31. Stroncek DF, Fellowes V, Pham C et al. Counter-flow elutriation of clinical peripheral blood mononuclear cell concentrates for the production of dendritic and T cell therapies. *J Transl Med.* 2014;12:241.
32. Martinez FO. Analysis of gene expression and gene silencing in human macrophages. *Curr Protoc Immunol.* 2012;96:14.28:14.28.1–14.28.23.
33. Narayan N, Mandhair H, Smyth E et al. The macrophage marker translocator protein (TSPO) is down-regulated on pro-inflammatory 'M1' human macrophages. *PloS one.* 2017;12:e0185767.
34. Liu H, Shi B, Huang C-C, Eksarko P, Pope RM. Transcriptional diversity during monocyte to macrophage differentiation. *Immunol Lett.* 2008;117:70-80.
35. Frede S, Stockmann C, Freitag P, Fandrey J. Bacterial lipopolysaccharide induces HIF-1 activation in human monocytes via p44/42 MAPK and NF-kappaB. *Biochem J.* 2006;396:517-27.
36. Krausgruber T, Blazek K, Smallie T et al. IRF5 promotes inflammatory macrophage polarization and TH1-TH17 responses. *Nat Immunol.* 2011;12:231-8.
37. Han J, Hajjar DP, Tauras JM, Feng J, Gotto AM, Jr., Nicholson AC. Transforming growth factor-beta1 (TGF-beta1) and TGF-beta2 decrease expression of CD36, the type B scavenger receptor, through mitogen-activated protein kinase phosphorylation of peroxisome proliferator-activated receptor-gamma. *J Biol Chem.* 2000;275:1241-6.

38. Ishida Y, Agata Y, Shibahara K, Honjo T. Induced expression of PD-1, a novel member of the immunoglobulin gene superfamily, upon programmed cell death. *EMBO J.* 1992;11:3887-95.
39. Butler DM, Feldmann M, Di Padova F, Brennan FM. p55 and p75 tumor necrosis factor receptors are expressed and mediate common functions in synovial fibroblasts and other fibroblasts. *Eur Cytokine Netw.* 1994;5:441-8.
40. Gent YY, Voskuyl AE, Kloet RW et al. Macrophage positron emission tomography imaging as a biomarker for preclinical rheumatoid arthritis: findings of a prospective pilot study. *Arthritis Rheumatol.* 2012;64:62-6.
41. Gent YY, Ter Wee MM, Voskuyl AE et al. Subclinical synovitis detected by macrophage PET, but not MRI, is related to short-term flare of clinical disease activity in early RA patients: an exploratory study. *Arthritis Res Ther.* 2015;17:266.
42. Buch MH, Vital EM, Emery P. Abatacept in the treatment of rheumatoid arthritis. *Arthritis Res Ther.* 2008;10:S5.
43. Frank-Bertoncelj M, Gay S. The epigenome of synovial fibroblasts: an underestimated therapeutic target in rheumatoid arthritis. *Arthritis Res Ther.* 2014;16:117.
44. Pilling D, Fan T, Huang D, Kaul B, Gomer RH. Identification of markers that distinguish monocyte-derived fibrocytes from monocytes, macrophages, and fibroblasts. *PloS one.* 2009;4:e7475.
45. Kunisch E, Fuhrmann R, Roth A, Winter R, Lungershausen W, Kinne R. Macrophage specificity of three anti-CD68 monoclonal antibodies (KP1, EBM11,

and PGM1) widely used for immunohistochemistry and flow cytometry. *Ann Rheum Dis.* 2004;63:774-84.

46. Canat X, Carayon P, Bouaboula M et al. Distribution profile and properties of peripheral-type benzodiazepine receptors on human hemopoietic cells. *Life Sci.* 1993;52:107-18.

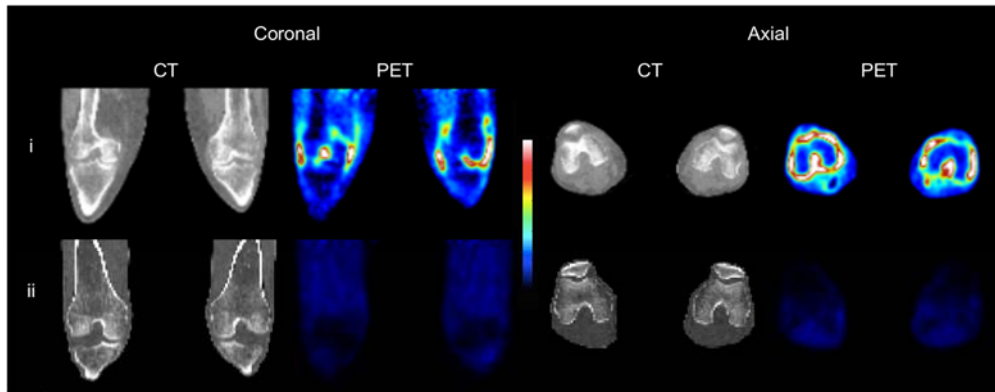
47. Notter T, Coughlin JM, Gschwind T et al. Translational evaluation of translocator protein as a marker of neuroinflammation in schizophrenia. *Mol Psychiatry.* January 17, 2017. (epub ahead of print).

48. Townsend MJ. Molecular and cellular heterogeneity in the Rheumatoid Arthritis synovium: clinical correlates of synovitis. *Best Pract Res Clin Rheumatol.* 2014;28:539-49.

49. Dennis G, Holweg CTJ, Kummerfeld SK et al. Synovial phenotypes in rheumatoid arthritis correlate with response to biologic therapeutics. *Arthritis Res Ther.* 2014;16:R90.

FIGURE LEGENDS

A



B

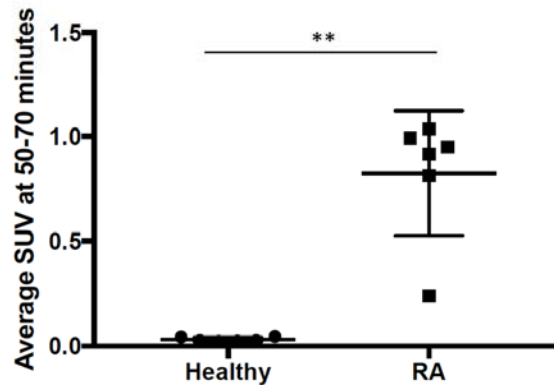


Figure 1 A: CT and ^{11}C -PBR28 PET SUV images both knees of (i) RA patient with clinical signs of synovitis both knees, (ii) healthy control. Colorimetric scale indicates red as maximal ^{11}C -PBR28 SUV, dark blue as minimal ^{11}C -PBR28 SUV. SUV was taken at 50-70 minutes post radioligand administration. **B:** comparison of ^{11}C -PBR28 SUV each knee in healthy controls and RA patients imaged (n=6 each group, **p<0.01 determined by Mann-Whitney U test).

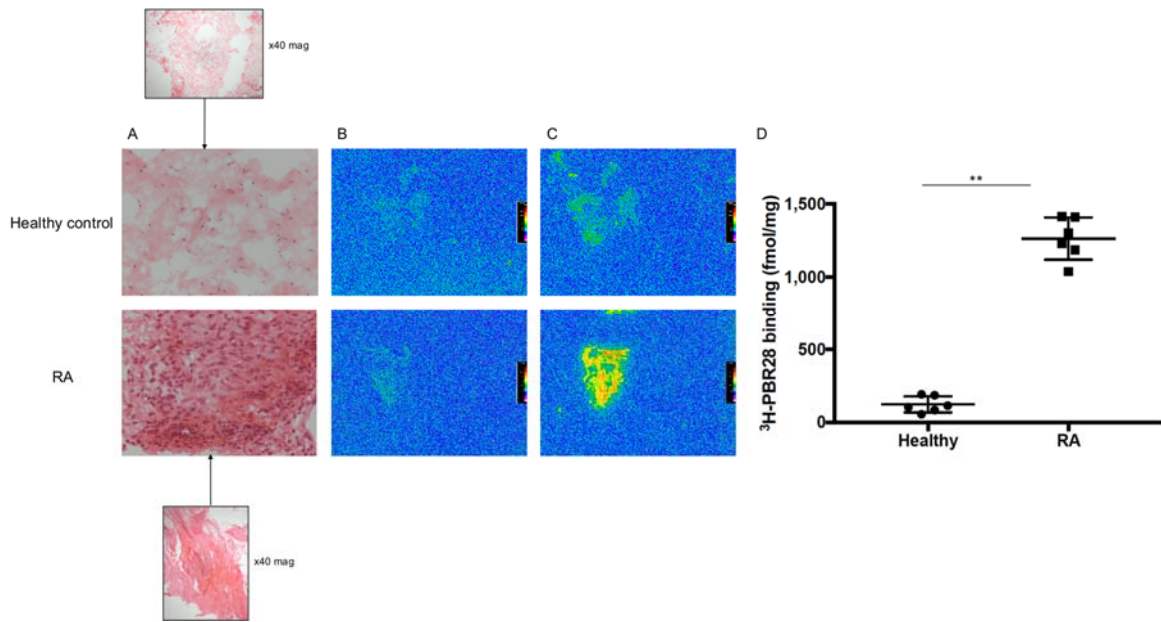


Figure 2 Autoradiography of synovial tissue **A:** Representative images of Haematoxylin and Eosin staining of synovial tissue (x400 magnification, scale bar=20 μ m) **B:** non-specific and **C:** total ³H-PBR28 binding for RA and healthy synovium x40 magnification, colorimetric scale indicates red as maximal ³H-PBR28 binding, blue minimal ³H-PBR28 binding. **D:** mean specific binding ³H-PBR28 in synovial tissue from 6 healthy controls and 6 RA patients, **p<0.01 as assessed by Mann-Whitney U test.

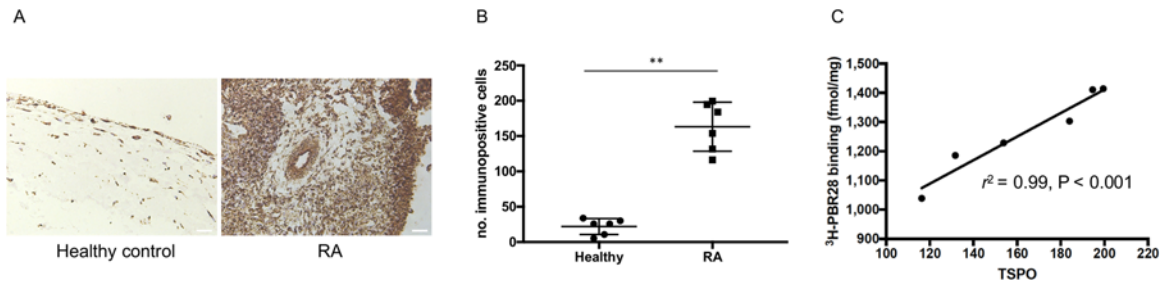


Figure 3 TSPO synovial tissue staining correlates with $^3\text{H-PBR28}$ binding **A**: Representative images of immunohistochemical staining of synovial tissue for TSPO, (x200 magnification, scale bar=50 μm). **B**: average number of immunopositive cells for TSPO immunohistochemical stain on serial sections of same 6 healthy controls and 6 RA synovial tissues used for autoradiography, $**p < 0.01$, as determined by Mann-Whitney U test. **C**: correlation between number of TSPO positive cells in RA synovial tissue sections (x axis), and average specific binding $^3\text{H-PBR28}$ from the same sections (y axis), $n=6$, $p < 0.001$ as assessed by Pearson's correlation.

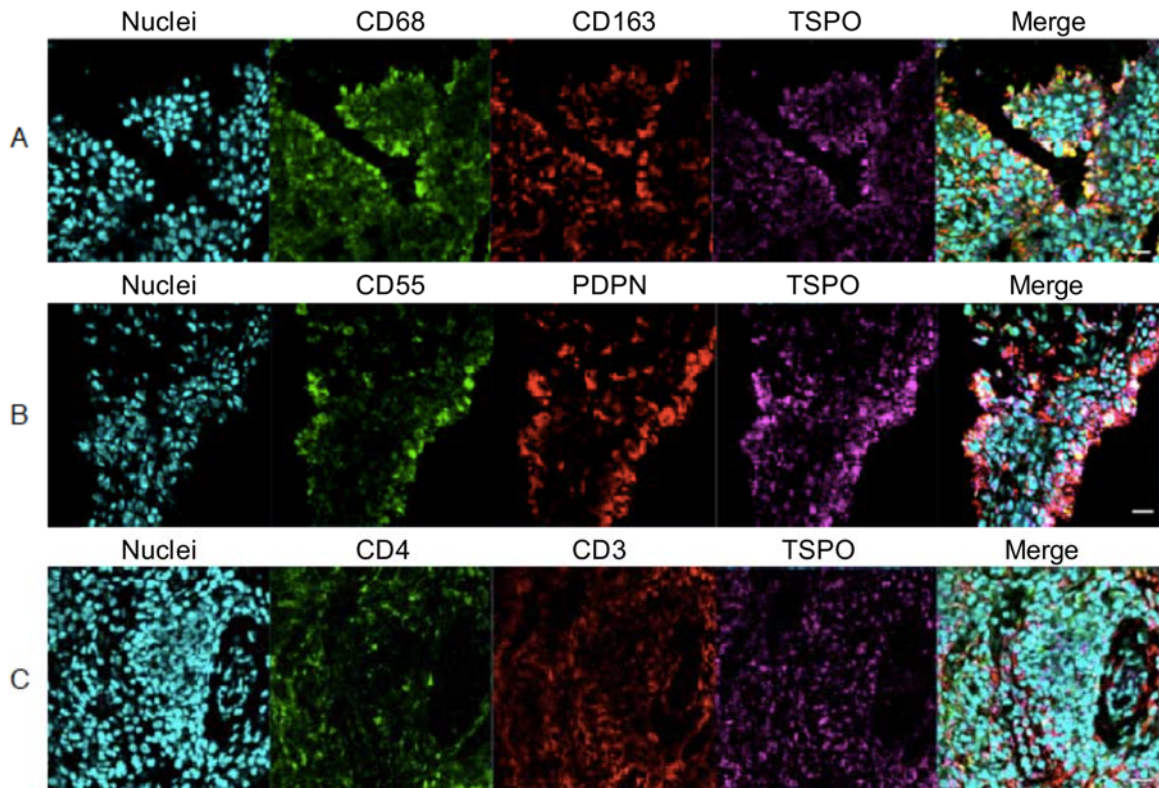


Figure 4 Representative confocal immunofluorescence images of RA synovial tissue demonstrating **A:** co-staining of macrophage markers CD68 (green), CD163 (red) with TSPO (purple) **B:** co-staining of FLS markers CD55 (green), PDPN (red) with TSPO (purple) **C:** co-staining of T cell markers CD4 (green), CD3 (red) with TSPO (purple). Nuclei were stained using POPO-1 (cyan). x400 magnification, scale bar=20 μ m.

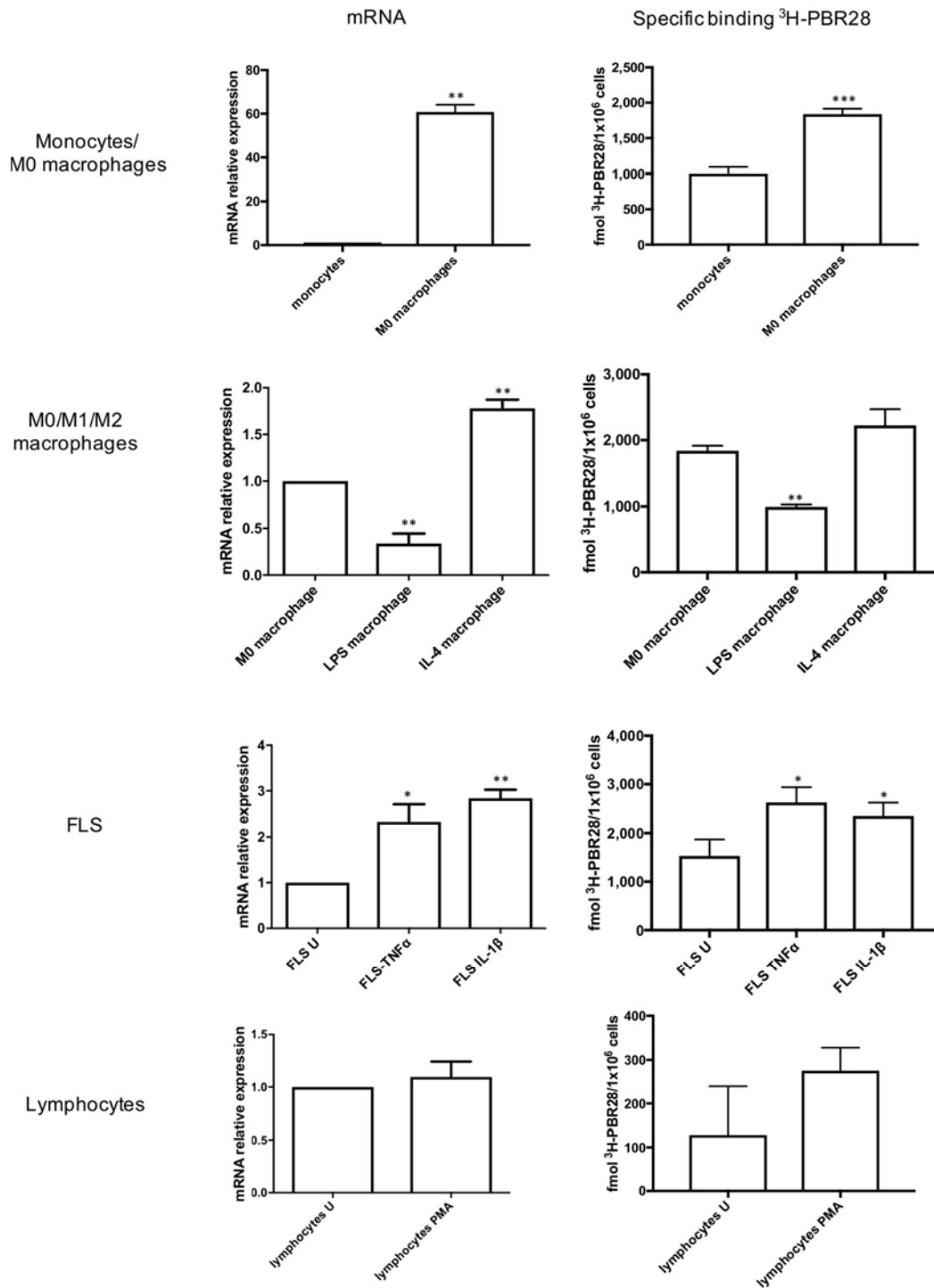


Figure 5 mean fold change *TSPO* mRNA expression (relative to unstimulated group) and mean specific binding of ³H-PBR28 in: monocytes and unstimulated 'M0' macrophages, M1 (M0 macrophages treated with 10ng/mL LPS and 20ng/mL

IFN- γ for 24 hours) and M2 macrophages (M0 macrophages treated with 20ng/mL IL-4 for 24 hours), unstimulated FLS (FLS U), FLS treated with 10ng/mL TNF- α , for 24 hours or treated with 10ng/mL of IL-1 β for 24 hours; unstimulated CD4+ T lymphocytes (lymphocytes U), and CD4+ T lymphocytes treated with 10ng/mL phorbol 12-myristate 13-acetate and 1 μ g/mL ionomycin for 6 hours (lymphocytes PMA). Data is expressed as mean \pm standard error of the mean of four independent experiments, with each experiment performed in triplicate. * p <0.05, ** p <0.01, *** p <0.001, as determined by Student t test, or one-way ANOVA with Bonferroni's multiple comparison test.

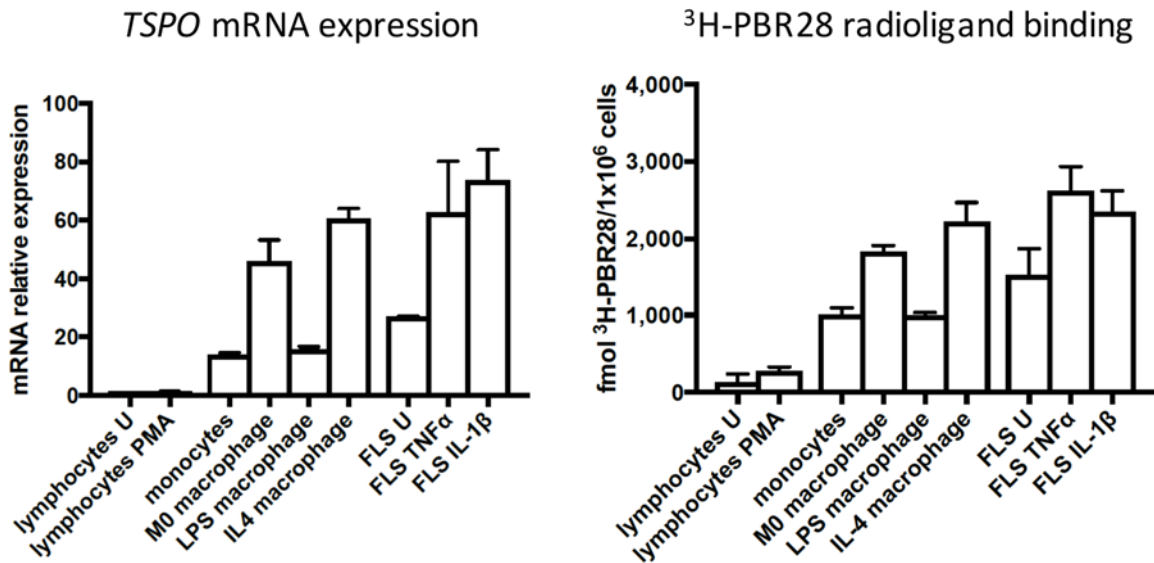


Figure 6 mRNA expression of *TSPO* in all cell groups, relative to unstimulated CD4+ T lymphocytes, and summary of ³H-PBR28 specific binding in all cell groups. Data is expressed as mean ± standard error of the mean of four independent experiments, with each experiment performed in triplicate. One way ANOVA, with Bonferroni's multiple comparison test used to compare *TSPO* expression between each group.

Supplemental data

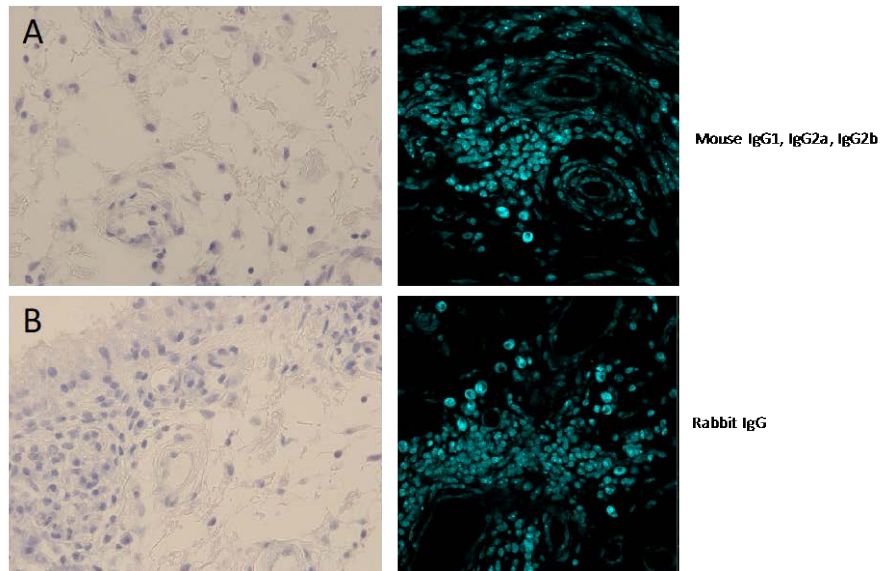
Participant	Age (years)	Medications (duration of administration at time of imaging and biopsy)
Participants with RA undergoing [¹¹ C]PBR28 imaging and providing synovial tissue from ultrasound guided biopsy.		
1	54	Methotrexate 15mg once weekly (2 weeks) Hydroxychloroquine 200mg twice daily (2 weeks) Folic acid 5mg once weekly (2 weeks)
2	52	Methotrexate 15mg once weekly (5 years) Folic acid 5mg once weekly (5 years) Prednisolone 5mg once weekly (12 months) Ketoprofen 200mg as needed (2 years)
3	43	Hydroxychloroquine 200mg twice daily (1 week)
Participants with RA providing synovial tissue from joint replacement surgery		
1	54	Methotrexate 20mg once weekly (5 years) Folic acid 5mg once weekly (5 years)
2	60	Methotrexate 15mg once weekly (3 years) Folic acid 5mg once weekly (3 years)
3	59	Leflunomide 20mg once daily (1 year)

Supplemental Table 1: Summary table of age of RA patients undergoing [¹¹C]PBR28 imaging, and providing synovial tissue for this work.

Antibody	Clone	Isotype	Species	Dilution for IF (for DAB IHC)
TSPO Abcam ab109497	EPR5384	IgG	Rabbit	1:1000 (1:10,000)
CD68 Dako M0814	KP-1	IgG1	Mouse	1:400 (1:4000)
CD163 LSBIO LS-C174770	34B	IgG2a	Mouse	1:2000 (1:2000)
PDPN GeneTex GTX585772	5E2	IgG2b	Mouse	1:1000 (1:1000)
CD55 LSBIO LS-C134498	Mab67	IgG1	Mouse	1:2000 (1:2000)
CD3 Abcam ab699	PS1	IgG2a	Mouse	1:50 (1:50)
CD4 LSBIO LS-C336492	IG10	IgG1	Mouse	1:400 (1:400)

Supplemental Table 2: Antibodies used for immunofluorescence and immunohistochemistry studies. IF=immunofluorescence, IHC=immunohistochemistry

Isotype controls for staining



isotype control staining of RA synovial tissue for all antibodies used in this study x400 magnification. Isotype controls for DAB IHC on the left, isotype controls for immunofluorescence on the right. **A:** isotype control staining for mouse antibodies (CD68, CD163, PDPN, CD3, CD4) **B:** isotype control staining for rabbit antibody used (TSPO).

Imaging acquisition for immunofluorescence studies.

Immunofluorescence images were acquired on a Zeiss LSM 710 confocal microscope using x40 oil immersion objective (Numerical Aperture=0.95). The fluorophores of POPO-1, Alexa Fluor 488, Alexa Fluor 568, and Alexa Fluor 633 were excited using the 405nm, 488nm, 561nm, and 633nm laser lines, respectively. To minimize bleed-through, all channels were acquired sequentially.